Supporting Information

for

Temperature-Driven Reaction Pathways in Direct Alkane Dehydrogenation over Metal-Free Nitrogen Doped Carbocatalysts

Jie Zhang[†a,b], Ranjan K. Behera[†b], Vy T. Nguyen[†c], Zhenhao Liu[b], Juan D. Jimenez[d], Kasala Prabhakar Reddy[d], Jorge Moncada[e,f], Cherno Jaye[e], Jinsu Oh[a], Chao Meng[a,b], Lin Zhou[a,b], Dr. Sanjaya D. Senanayake[d], Bin Wang*[c], Long Qi*[a,b], Wenyu Huang*[a,b]

[a] U.S. DOE Ames National Laboratory, Ames, IA, 50011, United States.

[b] Department of Chemistry, Iowa State University, Ames, Iowa 50011, United States.

[c] School of Sustainable Chemical, Biological and Materials Engineering, University of Oklahoma, Norman, OK 73019, United States.

[d] Chemistry Division, Brookhaven National Laboratory, Upton, NY, 11973, United States

[e] Material Measurement Laboratory, National Institute of Standards and Technology, Gaithersburg, MD 20899, United States

[f] National Synchrotron Light Source II, Brookhaven National Laboratory, Upton, New York 11973, United States

[†] These authors contributed equally to this work.

* Emails: lqi@iastate.edu; whuang@iastate.edu; wang_cbme@ou.edu

Table of content

Section 1. Experimental Procedures

1.1 Materials

Carbon tetrachloride (⩾99.9 %), Ethylenediamine (⩾99.5 %), Tetraethyl orthosilicate (TEOS, 98 %), and Pluronic P123 (Mn~5800) were purchased from Sigma-Aldrich. Hydrofluoric acid (TraceMetal grade), Hydrochloric acid (TraceMetal grade), Ethylbenzene (99.8 %, anhydrous), Styrene (99.5 %), and Methanol (99.8 %) were purchased from Thermo Fisher Scientific Inc. Per-deuterated ethylbenzene (98 %, D 97 %) and deuterated dimethyl sulfoxide (DMSO-d_6, 99.5 %, D 99.9 %) were purchased from Cambridge Isotope Laboratories. Helium (UHP Grade, 99.999 %), Argon (UHP Grade, 99.999 %), and Hydrogen (UHP Grade, 99.999 %) were purchased from Matheson Tri-gas, Inc. All chemicals were used as received.

1.2 Catalyst synthesis

Synthesis of mesoporous silica template SBA-15.

Pluronic P123 was first heated in a 70 °C oven until it melted. Then, 4 g of the viscous solution was transferred into a 500 mL sealed polypropylene bottle using a 50 mL syringe. To this, 120 mL of 2 mol/L hydrochloric acid and 30 mL of deionized water were added, and the mixture was stirred with a magnetic stirrer until fully dissolved. The solution was then heated and stirred in a water bath at 37 °C for 15 minutes. Subsequently, 8.5 g of TEOS was added to the solution, followed by continuous stirring for 20 h. The mixture was then transferred to an oven and heated at 100 °C for 24 h. The resulting white precipitate was collected and washed with approximately 1 liter of deionized water, followed by ≈250 mL of methanol. The wet solid was left to dry naturally in a fume hood for 2 days. Finally, the dried solid powder was heated to 550 °C in a muffle furnace at a ramp rate of 1 °C/min and calcined for 5 h. The final calcined product was obtained as the SBA-15 template.

Synthesis of Nitrogen assembly carbon (NAC) catalyst

The synthesis of the NAC catalyst follows our previously reported method.[1] Briefly, 2.0 mL of ethylenediamine was injected by syringe into a 50 mL single-neck round-bottom flask and stirred vigorously. Then, 2.5 mL of carbon tetrachloride was added, followed by stirring for 1 minute and sonication for another minute. Next, 800 mg of as-synthesized SBA-15 powder was introduced into the mixture. A condenser was attached, and the reaction was carried out in an oil bath at 90 °C overnight to facilitate condensation.

After the condensation step, the condenser was removed, and the mixture was heated at 120 °C for 12 h to eliminate any unreacted precursor. The resulting brown powder was then carbonized in a tube furnace under an argon flow (50 mL/min) with a heating ramp of 3 °C/min to 800 °C, where it was held for 2 h. The obtained black powder was subsequently etched with a mixture of 5% HF and 10% HCl aqueous solutions to remove the SBA-15 silica template. The catalyst was

recovered by centrifugation and washed ten times with deionized water. Finally, the purified catalyst was dried at 70 °C for future use.

1.3 Catalyst characterization.

Powder X-ray diffraction (XRD) patterns were collected with the 2 Theta angle range of (10 to 80)° on a Bruker D8 Advance Twin diffractometer using Cu Kα radiation (λ=1.541 Å). The accelerating voltage and current were 40 kV and 40 mA, respectively.

Nitrogen physisorption measurements were performed at -196.15 °C using a Micromeritics Tristar surface area and porosity analyzer. Before analysis, the samples were degassed at 200 °C for 4 h under Nitrogen flow. The total pore volume was determined from the total amount of N_2 vapor adsorbed at a relative pressure of 0.99. The specific surface area was calculated using the BET method. Pore size was estimated from the adsorption branch of the isotherm using the BJH method.

Inductively coupled plasma-mass spectrometry (ICP-MS) analysis was performed on an Agilent 7700 system. For sample preparation, 10 mg of catalyst powder was first calcined in a muffle furnace at 500 °C for 5 h to remove organic components. The resulting residue was then digested using a mixture of 1 mL concentrated nitric acid and 1 mL hydrofluoric acid. The solution was subsequently diluted to a final volume of 10 mL for analysis.

Ambient pressure X-ray photoelectron spectroscopy (AP-XPS): A commercial SPECS AP-XPS chamber equipped with a PHOIBOS 150 EP MCD-9 analyzer in the Chemistry Division of Brookhaven National Laboratory was used for AP-XPS measurements. The Gold $4f_{7/2}$ peak at 84.0 eV was used for energy calibration of the spectra using an Au (111) single crystal. Powder samples were pressed onto a roughened aluminum plate and loaded into the APXPS chamber. Measurements were conducted either at UHV conditions (≈1.0×10^{-7} Pa) or in the presence of 2.7 x 10^3 Pa H_2, samples were brought to temperature via radiative heating with a halogen bulb. All measurements were done using an Al kα X-Ray source (1486.61 eV) using a pass energy of 50 eV, 20 scans, and a dwell time of 0.1 sec.

Near-edge X-rays Absorption Fine Structure (NEXAFS) studies were performed in the National Synchrotron Light Source II of Brookhaven National Laboratory. The powdered samples were mounted on an aluminum bar using a conductive adhesive before loaded them in an ultra-high vacuum (UHV) experimental chamber. NEXAFS measurements were performed in partial electron yield mode (PEY) with a detector entrance grid voltage of -150 Vdc; as well as fluorescence yield (FY) and total electron yield (TEY) modes. An elliptically polarized undulator X-ray source monochromatized by a 1200 lines/mm varying line spacing plane grating monochromator and a 25-μm exit slit provided an energy resolution of about 0.1 eV at the C and N *K*-edges. To correct for any beam intensity fluctuations due to the source or beamline optics, the spectra intensity was normalized to the drain current intensity of a clean gold mesh located immediately upstream of the experimental chamber. A simultaneous measurement of the carbon and nitrogen absorption spectra respectively of a carbon mesh and a titanium nitride mesh located

further upstream was used to monitor any beam energy shifts during the measurements.

Scanning Transmission Electron Microscopy (STEM) images were collected on a JEOL 2100 STEM, equipped with a basic STEM, a Thermo Fisher Scientific Pinnacle System light-element energy dispersive x-ray spectrometer (EDS), and a Gatan OneView 4K digital camera for image recording. The images were collected at the operating voltages of 200 kV.

Aberration-corrected Scanning Transmission Electron Microscope (STEM) images and Electron Energy Loss Spectroscopy (EELS) analysis were recorded on an FEI Titan Themis cubed probe aberration-corrected STEM, operating at 200 kV.

1.4 Reaction Studies

Direct dehydrogenation of ethylbenzene studies

The ethylbenzene dehydrogenation reactions were conducted in a fixed-bed continuous-flow reactor. In a typical experiment, 20 mg of the NAC catalyst was diluted with 1.00 g of quartz sand at a 1:50 ratio. All reactions were conducted in a U-shaped high-purity quartz tube reactor to eliminate potential metal contamination, and a blank test without catalyst (quartz wool and quartz sand only) showed only ~1% ethylbenzene conversion under otherwise identical conditions. Prior to the reaction, the catalyst was pretreated by flowing helium (He) at 50 mL/min for 30 minutes. Unless otherwise specified, all reactions were performed under hydrogen-free conditions. The total flow rate of gaseous reactants was maintained at 50 mL/min using mass flow controllers (Alicat), consisting of 2.5 mL/min of He passing through a bubbler containing ethylbenzene (EB) and 47.5 mL/min of He as the balance gas, resulting in an actual EB flow of 0.15 μL/min. The EB vapor was introduced into the reaction stream by bubbling He through liquid EB maintained at 25 °C. To prevent condensation on the catalyst surface, the EB feed was bypassed through the reactor until the temperature reached 150 °C. All pipelines were maintained at 150 °C using heating tape to prevent condensation.

Catalyst activity was evaluated over a temperature range of (150 to 550) °C. Reaction products were analyzed online using a gas chromatograph (HP 5890 GC) equipped with a six-way valve and heated transfer lines. Gaseous products were quantified using a flame ionization detector (FID). The carbon balance for all catalytic studies was within ±4 %. Conversion of ethylbenzene (X_{EB}), selectivity of styrene (S_{ST}) product and carbon balance were calculated as follows:

$$X_{EB} = \left[\frac{Ethylbenzene_{in} - Ethylbenzene_{out}}{Ethylbenzene_{in}}\right] \text{x } 100\%$$

$$S_{EB} = \left[\frac{Styrene_{out}}{Ethylbenzene_{in} - Ethylbenzene_{out}}\right] \text{x } 100\%$$

$$Carbon\ balance = \left[\frac{Ethylbenzene_{out} + Styrene_{out}}{Ethylbenzene_{in}}\right] \text{x } 100\%$$

Kinetic Studies

To minimize mass transport limitations, all conversions were maintained below 10% while determining the kinetic parameters of the ethylbenzene dehydrogenation reaction. The reaction order studies were conducted using the same continuous-flow gas-phase reactor described earlier. The rate orders with respect to ethylbenzene were determined by varying the ethylbenzene and H_2 flow rates while maintaining constant reaction temperatures of 300 °C (for low-temperature conditions) and 500 °C (for high-temperature conditions).

Isotope Labelling Studies

Isotope labeling experiments were conducted to investigate the ethylbenzene dehydrogenation mechanism. These studies were performed in a fixed-bed gas-phase reactor connected to a mass spectrometer (MSD 5973). In a typical experiment, 20 mg of NAC catalyst, diluted with quartz sand, was packed into a U-tube reactor and pretreated at 150 °C for 1 hour under a helium flow of 50 mL/min. Following pretreatment, the reactant feed, consisting of 30.0 mL/min He, 17.5 mL/min H_2, and 2.5 mL/min He passing through a bubbler containing ethylbenzene-d_{10}, was introduced into the reactor. The reactor outlet was connected to both the mass spectrometer and a sample collection vial containing 2.0 mL of DMSO-d_6. The extent of H/D exchange was analyzed using ^{1}H and ^{13}C NMR for all samples collected in DMSO-d_6. In the NMR spectra, the solvent peak appeared at approximately 2.5 μL/L, while the water peak was observed at around 3.35 μL/L. The assignment of NMR signals for styrene and ethylbenzene is based on data from authentic samples and results from the literature.[2]

1.4 Theoretical Studies

Density functional theory (DFT) calculations of ethylbenzene dehydrogenation on NAC were conducted using the Vienna Ab initio Simulation Package (VASP).[3] The exchange and correlation energies were described using the functional proposed by Perdew, Burke, and Ernzerhof,[4] based on the generalized gradient approximation (GGA). Electron-core interactions were treated with the projector augmented wave (PAW) method.[5]

The computational model consisted of a single graphene sheet containing approximately 160 carbon atoms and (2 to 4) nitrogen atoms, consistent with our previous studies.[1, 6], [7] The supercell dimensions were 19.65 Å × 21.27 Å, with a vacuum spacing of 20 Å to prevent interactions between periodic images. Atomic structures were fully relaxed for H_2 dissociation barrier calculations. A kinetic energy cutoff of 400 eV was applied, and the Brillouin zone was sampled at the Gamma point with a single k-point.

Minimum energy pathways were determined using the climbing image nudged elastic band (CI-NEB) method and the dimer method.[8] Transition states were further validated by vibrational frequency calculations.

Section 2. Supplementary Figure and Tables

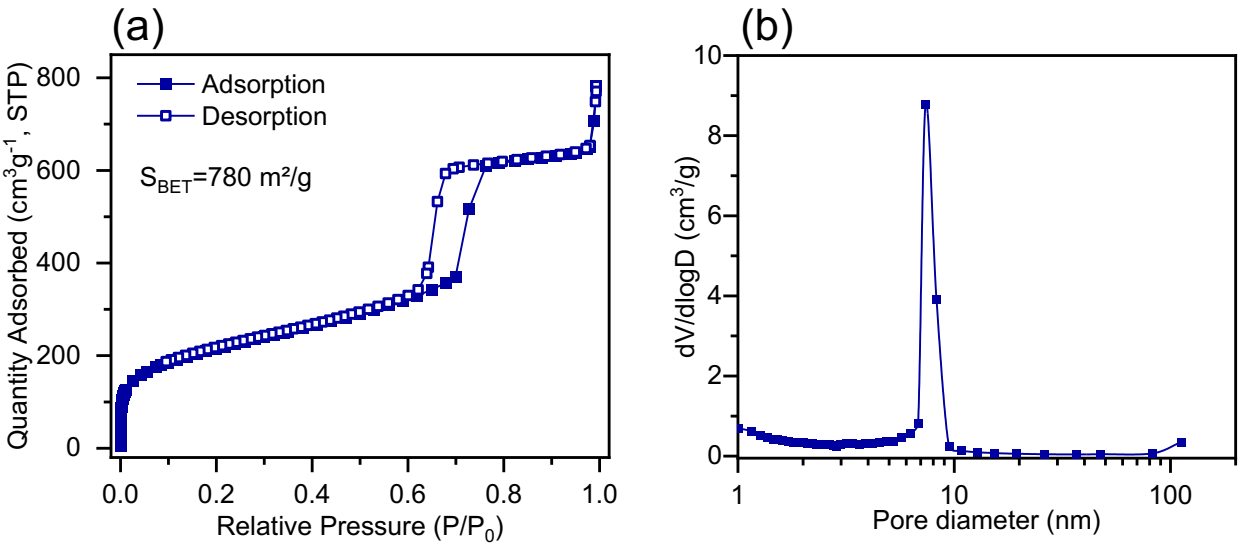

Figure S1 N_2 physisorption isotherms (a) and pore size distributions (b) of as-synthesized SBA-15 silica.

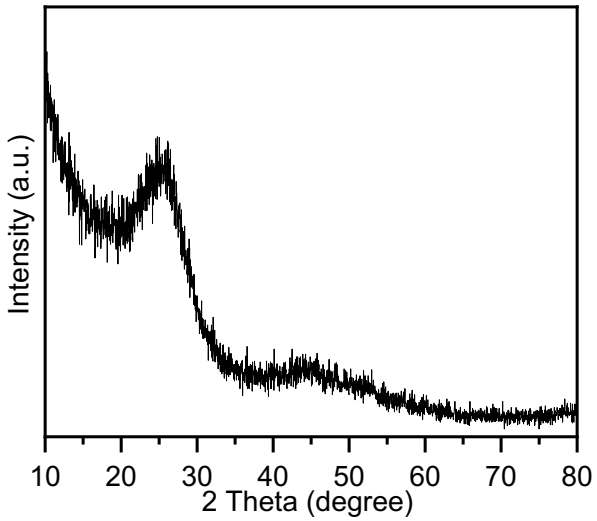

Figure S2 XRD patterns of NAC catalyst. Intensity is reported in arbitrary units (a.u.).

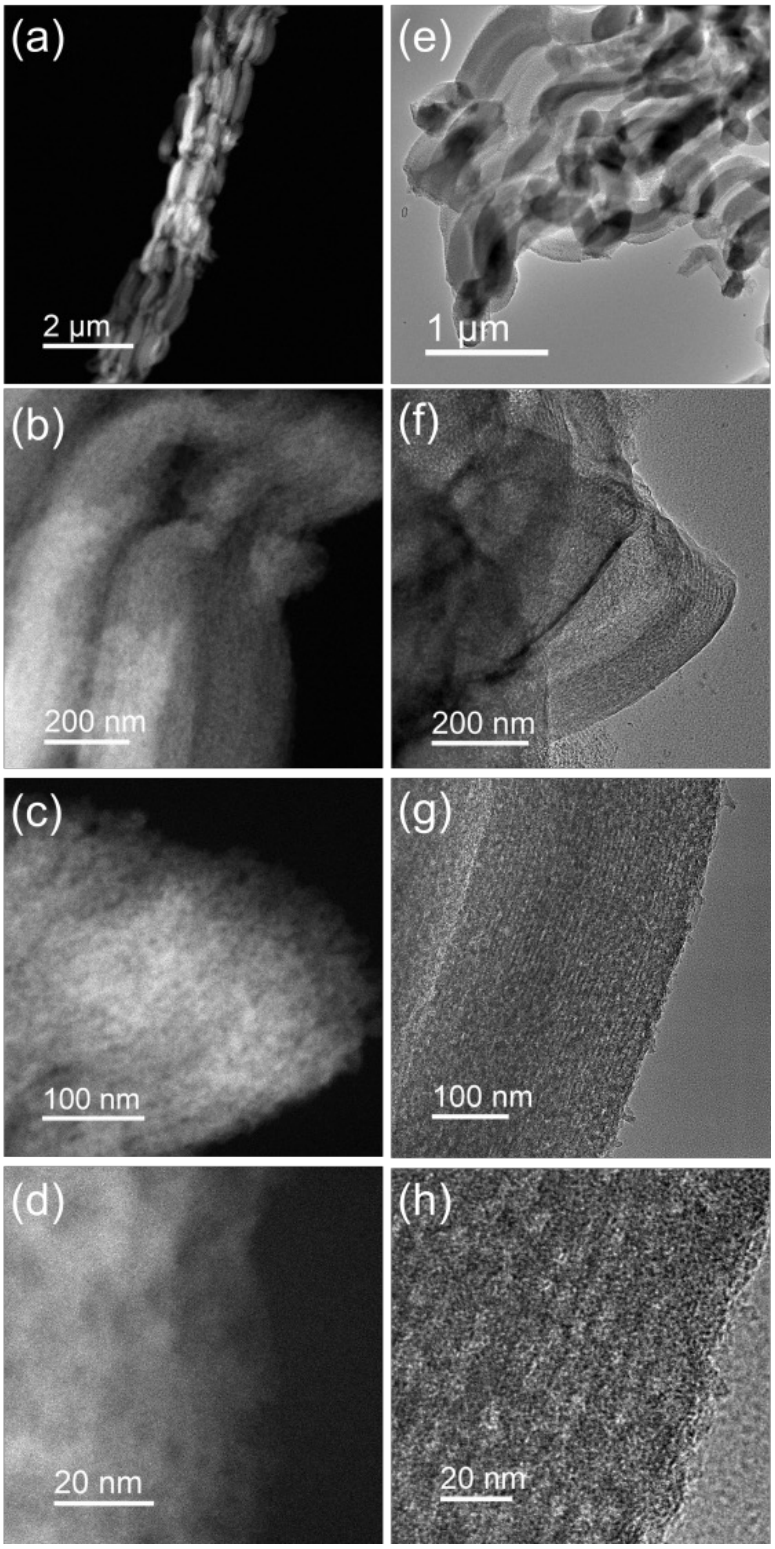

Figure S3 High angle annular dark field (HAADF, a-d) scanning transmission electron microscopy and bright field (BF, e-h) transmission electron microscopy images of the NAC catalyst.

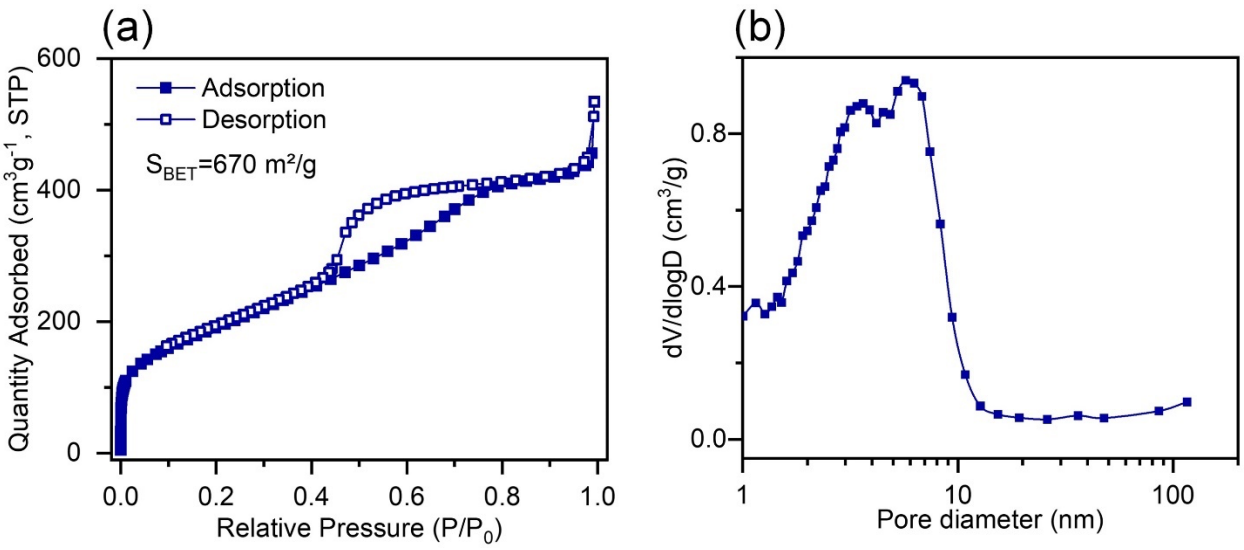

Figure S4 N_2 physisorption isotherms (a) and pore size distributions (b) of NAC catalyst.

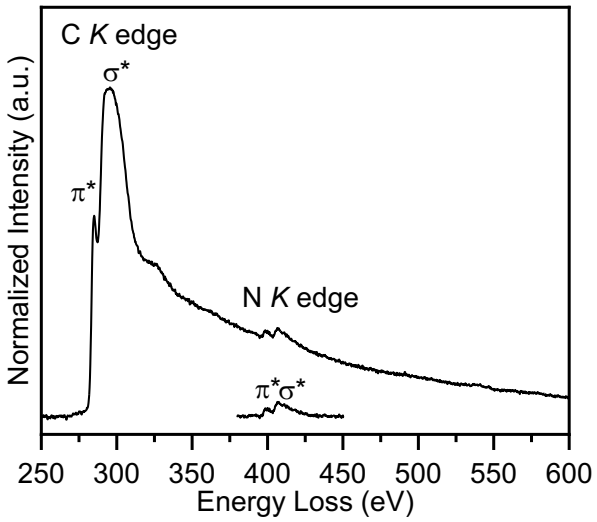

Figure S5 Electron energy loss spectroscopy (EELS) spectra of the fresh NAC catalyst.

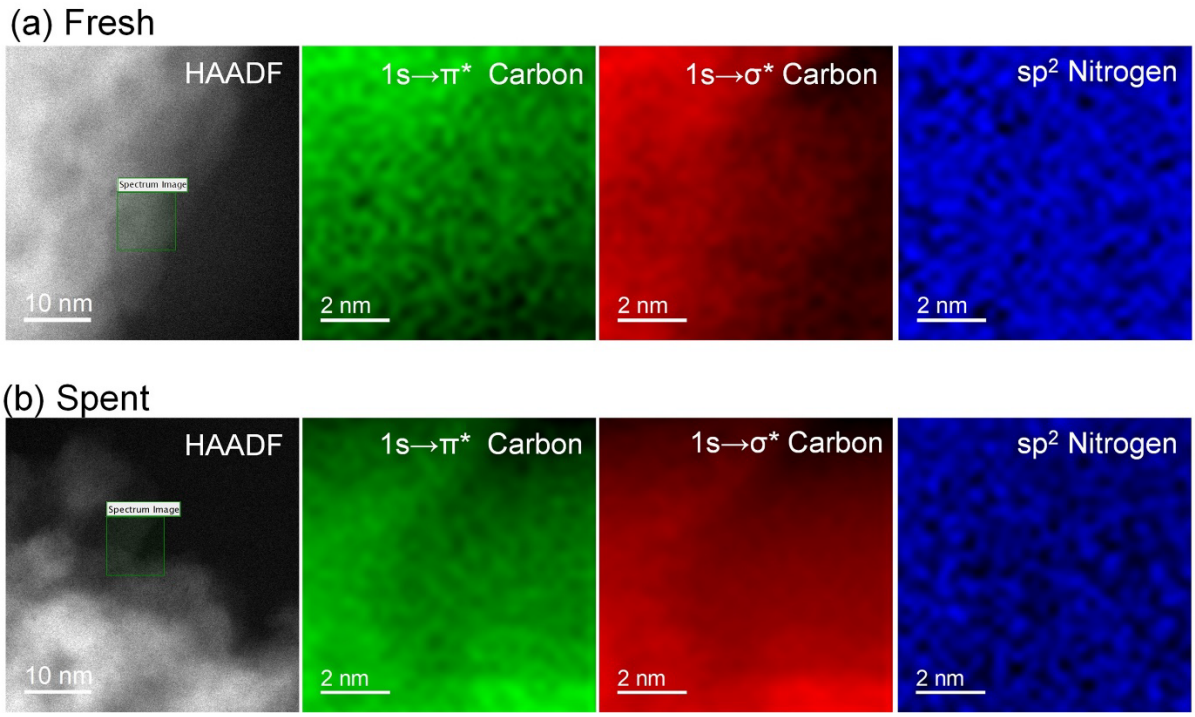

Figure S6 EELS mapping of the fresh (a) and spent (b, after a 120-hour EB dehydrogenation reaction) NAC catalyst. Colorized elemental maps of NAC at the range of (281.0 to 286.0) eV (in green) induced by transitions to the π* molecular orbital due to the presence of sp^2 bonding, at the range of (286.0 to 308.0) eV (in red) induced by transitions to σ* orbitals due to both sp^2 and sp^3 hybrid orbitals of carbon, and at the range of (396.8 to 421.5) eV (in blue) induced by transitions to 2p orbitals of nitrogen.

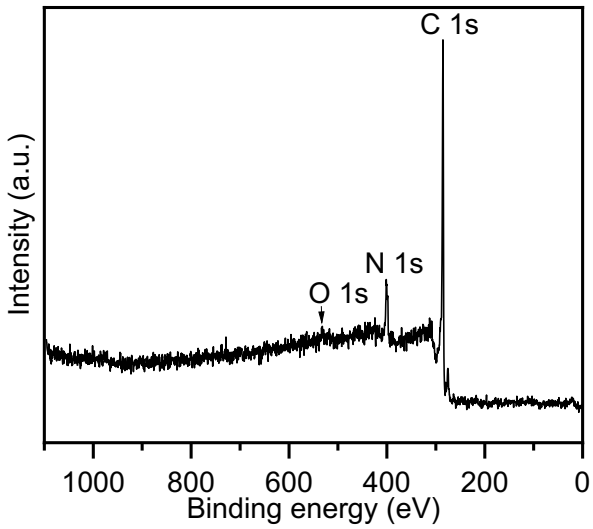

Figure S7 Wide XPS survey spectra of NAC catalyst. No obviously metal impurities except C, N and O signals can be observed from wide survey spectra.

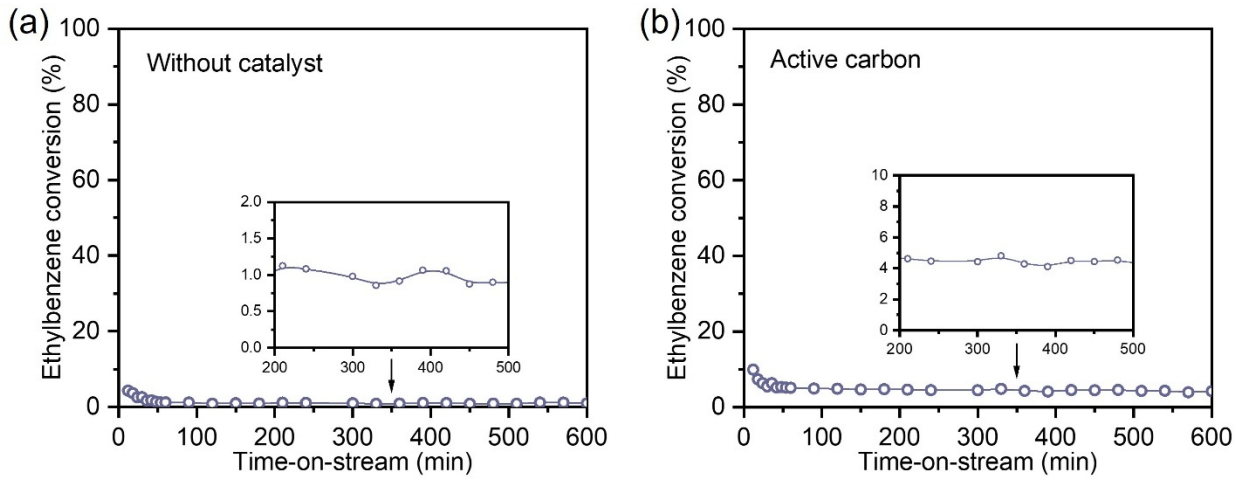

Figure S8. Time-on-stream performance for the direct dehydrogenation of ethylbenzene over (a) a blank reactor (no catalyst) and (b) activated carbon (AC, CABOT BLACK PEARLS 2000, GP-3632, surface area ~1500 $m^2 \cdot g^{-1}$). Conditions: (a) ethylbenzene partial pressure, 56 Pa; He, 50 $ml \cdot min^{-1}$ (STP); 550 °C. (b) AC, 8.8 mg; ethylbenzene partial pressure, 56 Pa; WHSV of 0.2 $g_{EB} \cdot g_{cat}^{-1} \cdot h^{-1}$; He 50 $mL \cdot min^{-1}$ (STP); 550 °C.

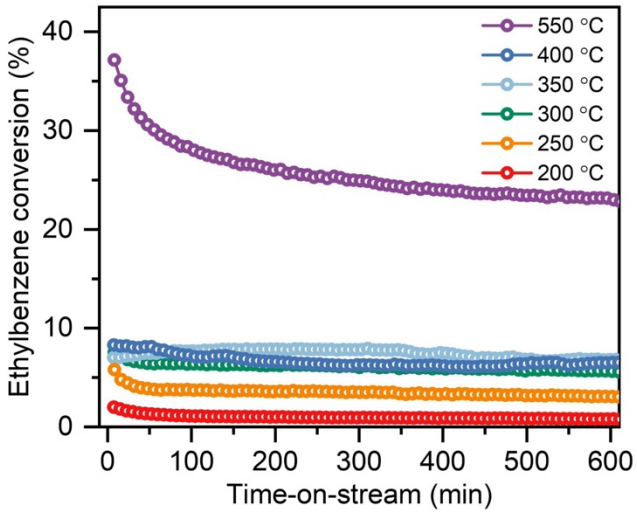

Figure S9 Time-on-stream studies of direct dehydrogenation of ethylbenzene at different temperatures over the NAC catalyst. Conditions: catalyst 20 mg, ethylbenzene 56 Pa, WHSV of 0.4 $g_{EB} \cdot g_{cat}^{-1} \cdot h^{-1}$, and He 50 $mL \cdot min^{-1}$ (STP).

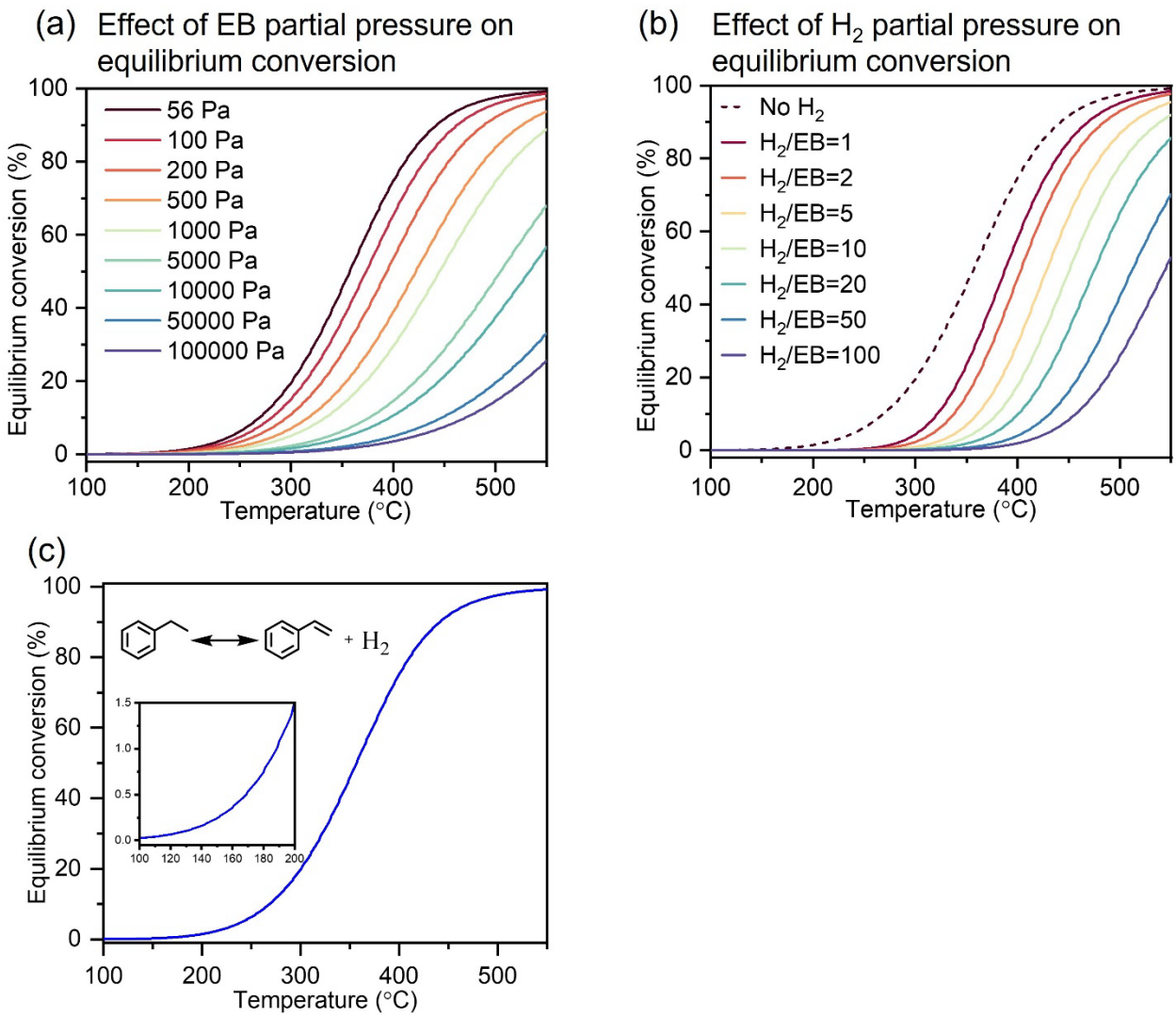

Figure S10 Equilibrium conversion of ethylbenzene. (a) Conditions: total pressure 0.1 MPa; initial gas mixture of ethylbenzene and He; ethylbenzene partial pressure 56-100000 Pa; temperature range 100-550 °C.(b) Conditions: total pressure 0.1 MPa; initial gas mixture of ethylbenzene, He, and added H_2; ethylbenzene partial pressure 56 Pa; H_2 partial pressure 56-5600 Pa; temperature range 100-550 °C. (c) Conditions: Total pressure of 0.1 MPa, ethylbenzene partial pressure of 56 Pa.

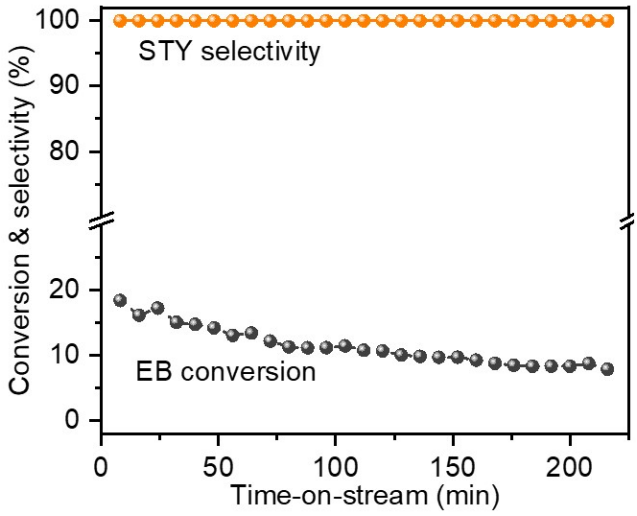

Figure S11 Direct dehydrogenation of ethylbenzene at a long contact time over NAC catalyst. Conditions: catalyst 120 mg, ethylbenzene 56 Pa, WHSV of 0.07 $g_{EB} \cdot g_{cat}^{-1} \cdot h^{-1}$, He 50 $mL \cdot min^{-1}$ (STP), and 300 °C.

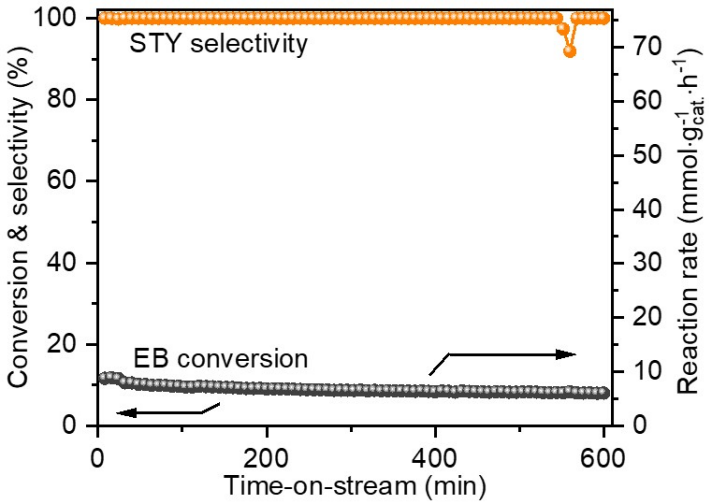

Figure S12 Direct dehydrogenation of ethylbenzene at a long contact time over NAC catalyst. Conditions: catalyst 2 mg, ethylbenzene 56 Pa, WHSV of 8.0 $g_{EB}·g_{cat}^{-1}·h^{-1}$, He 50 $mL·min^{-1}$ (STP), and 550 °C.

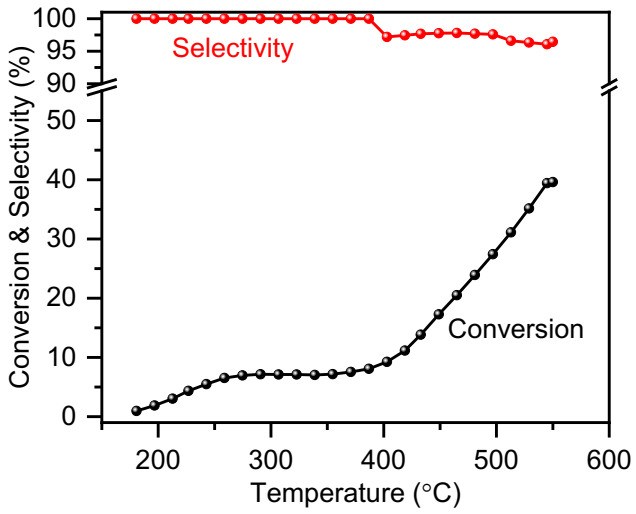

Figure S13 Temperature programmed reaction of ethylbenzene direct dehydrogenation over the NAC catalyst. Conditions: catalyst 20 mg, ethylbenzene 56 Pa, WHSV of 0.4 $g_{EB} \cdot g_{cat}^{-1} \cdot h^{-1}$, and He 50 $mL \cdot min^{-1}$ (STP) with a temperature ramping rate of 2 °C/min.

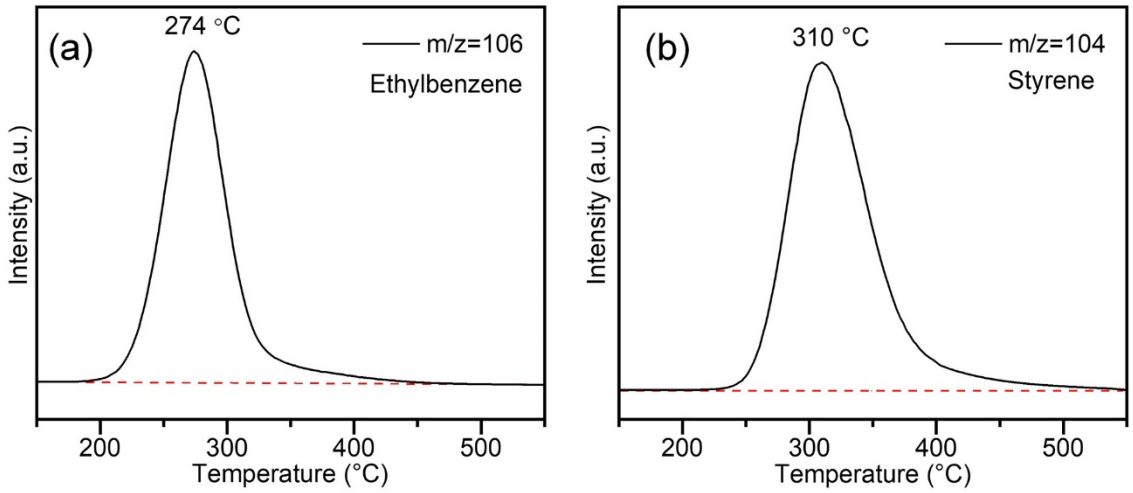

Figure S14 Temperature-programmed desorption analysis of ethylbenzene (a) and styrene (b) adsorbed on the NAC catalyst. Adsorption occurred at 150 °C for 30 min, followed by 150 min of He flow to remove physiosorbed species. TPD was performed by heating to 550 °C at a ramping rate of 20 °C/min.

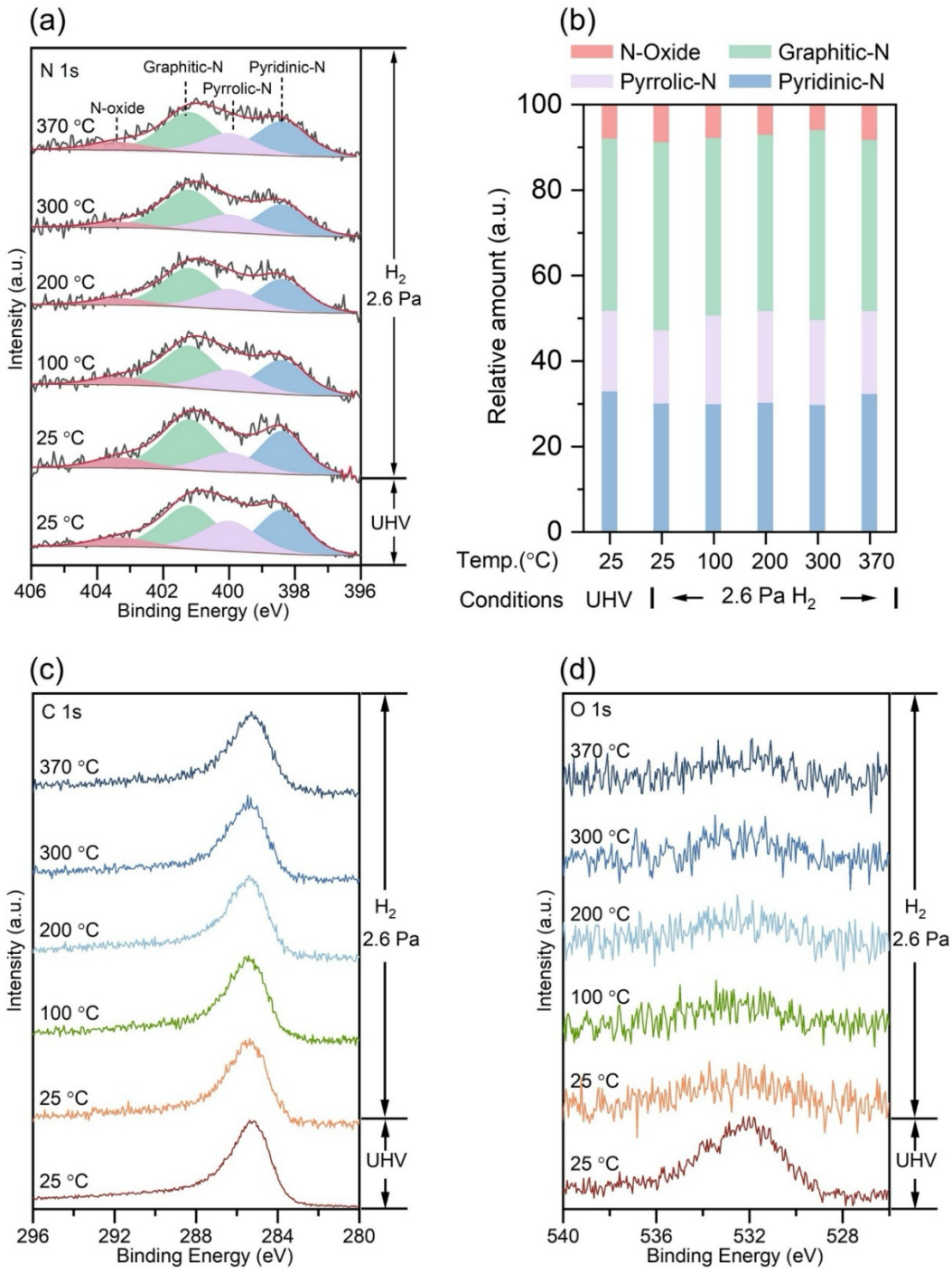

Figure S15. Effect of hydrogen on nitrogen sites on the NAC catalyst. The AP-XPS results of N 1s (a), C 1s (c), and O 1s (d) for the NAC catalyst exposed to 2.6 Pa of hydrogen at various temperatures after pre-treatment in UHV conditions at 400 °C. (b) The relative nitrogen ratio with temperature under UHV and hydrogen treatment. The changes to the relative nitrogen ratio are minimal and within the uncertainty of XPS curve fitting.

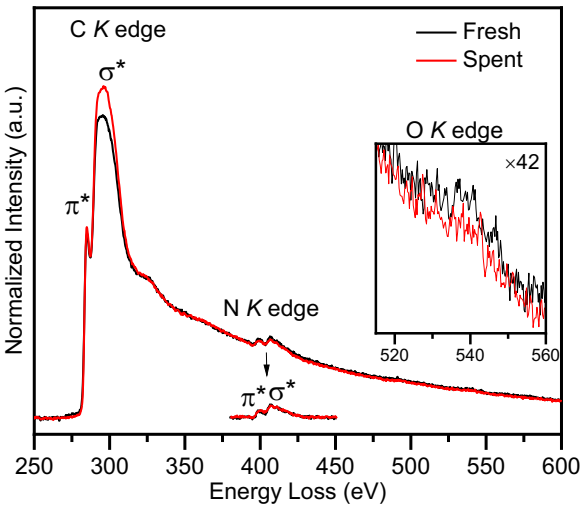

Figure S16. EELS spectra of the NAC catalyst before (fresh) and after (spent) a 120-hour of time-on-stream study of ethylbenzene dehydrogenation. The spectra show the C, N, and O K-edges. At the C K edge, the π* peak (≈285 eV) corresponds to sp^2-hybridized carbon.

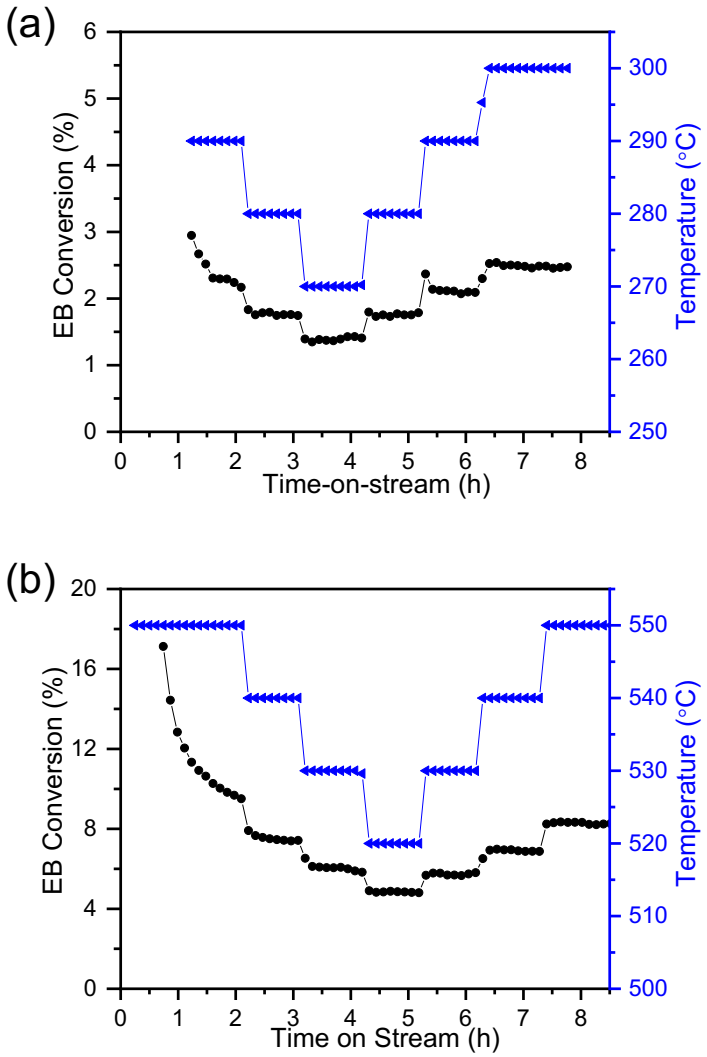

Figure S17 Calculated Arrhenius plots for NAC catalyst at (a) low temperature (270 to 300) °C and (b) high temperature range (520 to 550) °C. Conditions: catalyst 10-20 mg, ethylbenzene 56 Pa, ethylbenzene feeding rate of 0.15 μL·min^{-1}, and He 50 mL·min^{-1} (STP). The ethylbenzene conversion was controlled to be lower than 10 % for the high-temperature range and 5 % for the low-temperature range, which are far lower than the equilibrium conversion.

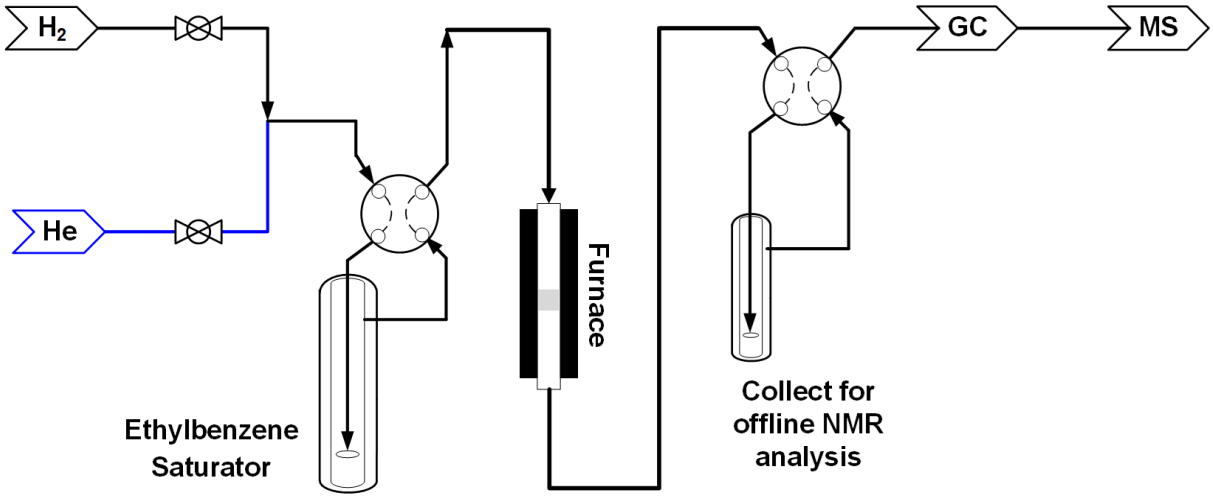

Figure S18 Schematic of the experimental setup for isotope labeling experiments, detailing the cascade detection methods (see also Figure 3 in the main manuscript).

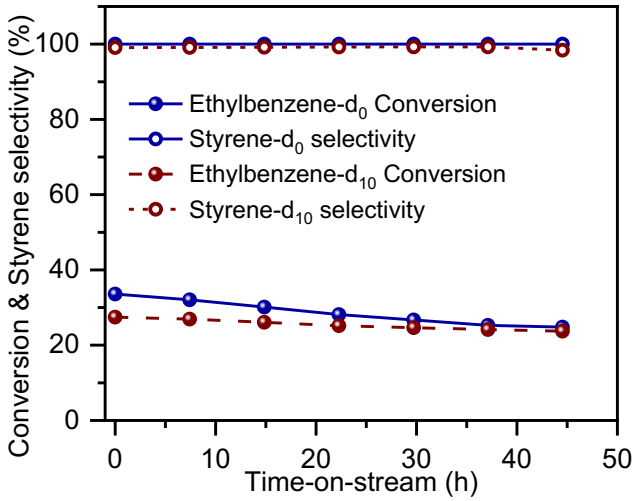

Figure S19 Comparison of catalytic performance for the dehydrogenation of deuterated vs. non-deuterated (naturally abundant) ethylbenzene over the NAC catalyst. Conditions: catalyst 20mg, ethylbenzene 56 Pa, WHSV of 0.4 $g_{EB} \cdot g_{cat}^{-1} \cdot h^{-1}$, He 32.5 $mL \cdot min^{-1}$ (STP), and H_2 17.5 $mL \cdot min^{-1}$ (STP), 550 ºC.

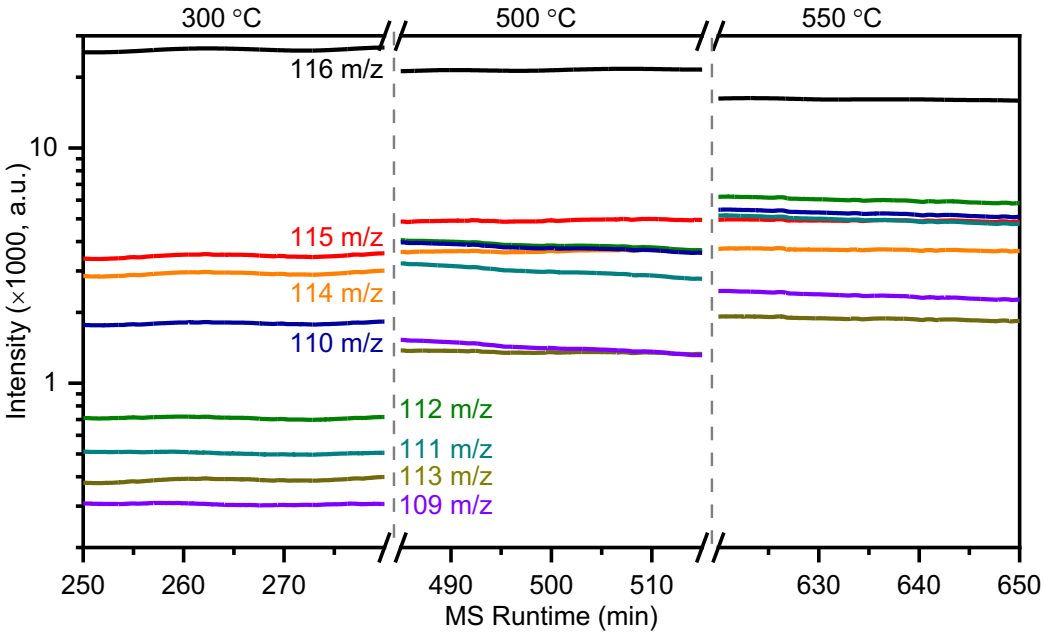

Figure S20 In-situ MS spectra analysis of the ethylbenzene-d_{10} co-react with hydrogen gas over the NAC catalyst at different temperatures. Conditions: catalyst 20 mg, ethylbenzene-d_{10} of 56 Pa, WHSV of 0.4 $g_{EB} \cdot g_{cat}^{-1} \cdot h^{-1}$, He 32.5 $mL \cdot min^{-1}$ (STP), and H_2 17.5 $mL \cdot min^{-1}$ (STP).

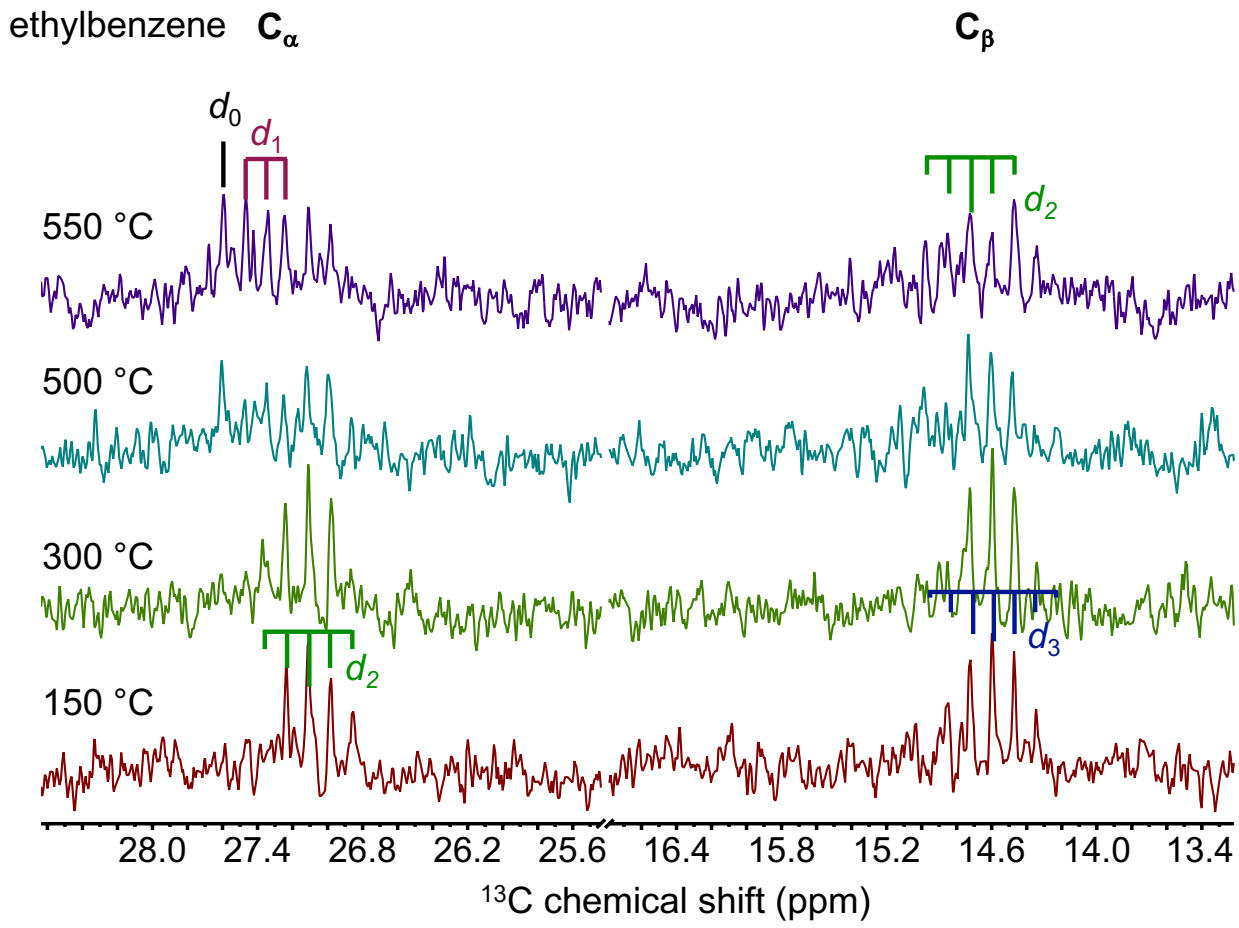

Figure S21 *Ex situ* ^{13}C NMR spectra analysis of partially 1H-exchanged ethylbenzene-d_{10} in the effluent products from the ethylbenzene-d_{10} dehydrogenation reaction over the NAC catalyst at variable temperature in the presence of hydrogen. Only the NMR regions for ethylbenzene α and β positions are shown. Conditions: catalyst 20.0 mg, ethylbenzene-d_{10} 56 Pa, WHSV of 0.4 $g_{EB} \cdot g_{cat}^{-1} \cdot h^{-1}$, He 32.5 mL·min^{-1} (STP), and H_2 17.5 mL·min^{-1} (STP).

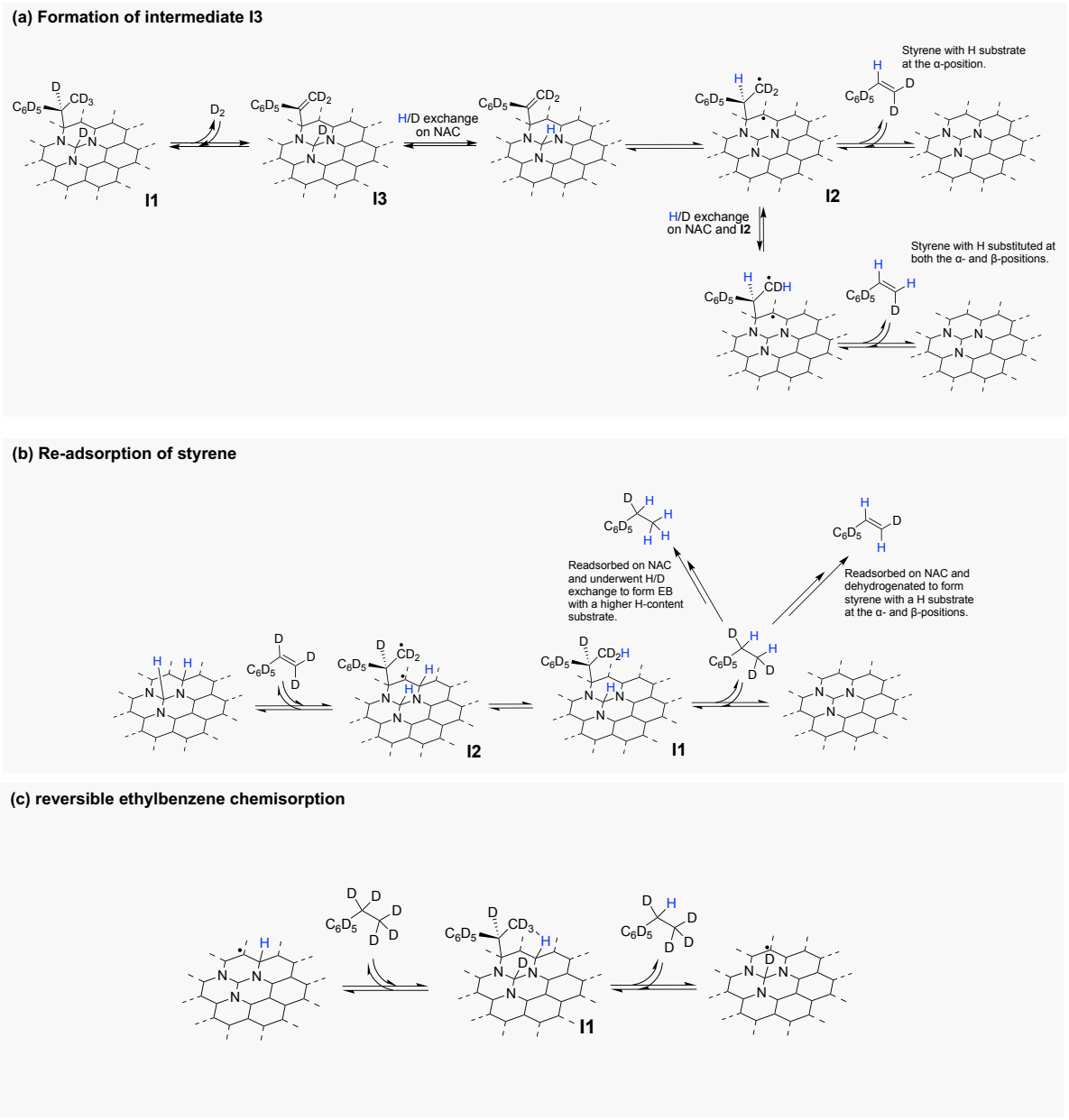

Figure S22 Illustration of the proposed pathways for H/D exchange at 500 °C and 550 °C. (a) Pathway 1 via formation of intermediate **I3**, which subsequently converts to styrene via H/D exchange at the α-position; (b) Pathway 2 via re-adsorption of styrene on the NAC surface, leading to the formation of ethylbenzene and styrene with H/D exchange at the α-position; and (c) Pathway 3 via reversible ethylbenzene chemisorption.

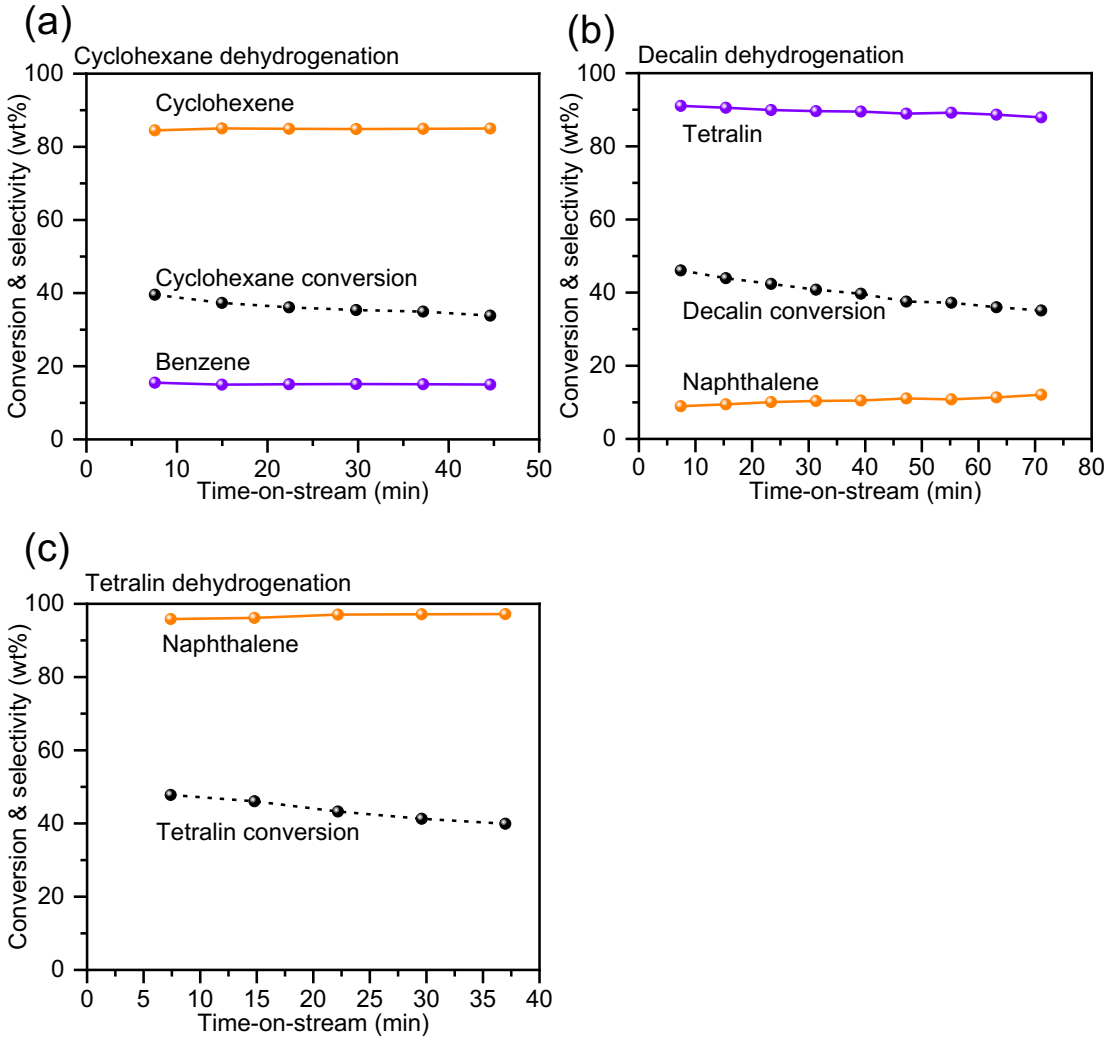

Figure S23 Substrate scope study for direct dehydrogenation of (a) cyclohexane, (b) decalin, and (c) tetralin. Conditions: 10 mg catalyst, 550 °C temperature, 5 mL·min^{-1} helium through a saturator for alkane substrates, and a total helium flow rate of 50 mL·min^{-1}.

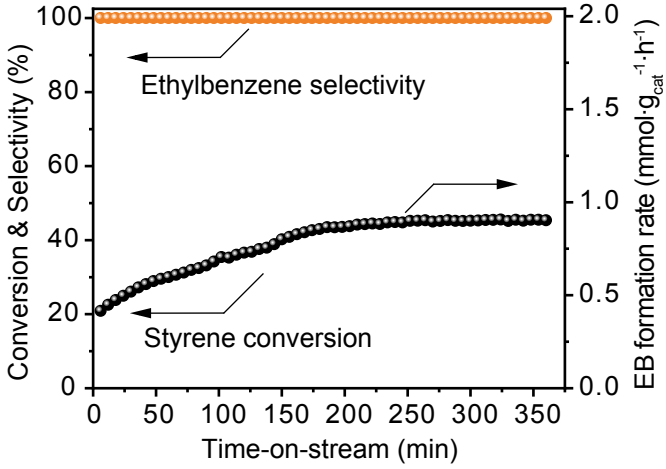

Figure S24 Styrene hydrogenation over the NAC catalyst. Conditions: 20 mg catalyst, 250 °C, total gas flow rate = 5.6 mL/min with a gas composition of H_2/He = 3.7/1.9 mL/min, Styrene = 0.078μL/min, corresponding to an H_2: Styrene molar ratio of 223:1. The WHSV of styrene is 0.21 $g_{styrene}·g_{cat.}^{-1}·h^{-1}$.

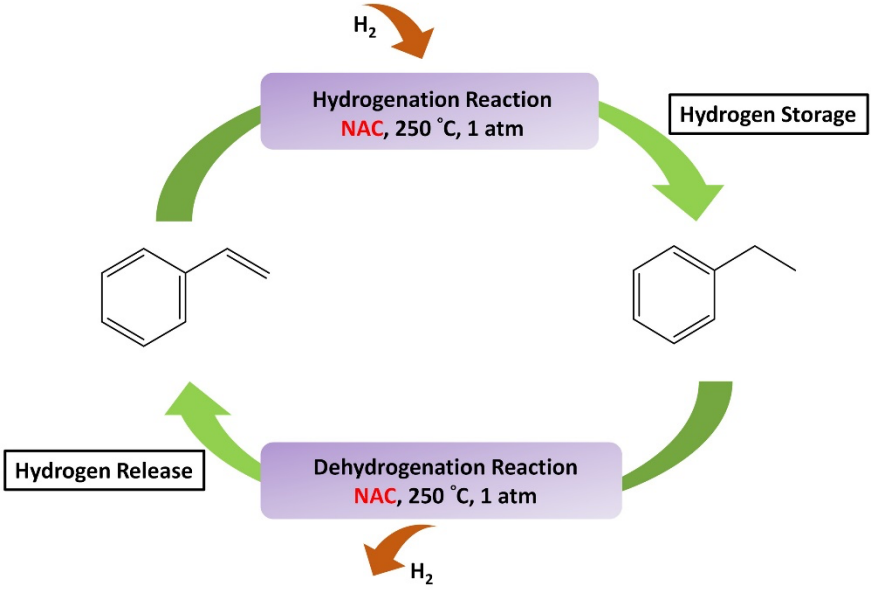

Figure S25 Illustration of the hydrogenation and dehydrogenation processes for the ethylbenzene–styrene.

Table S1 The measurement of trace metals in ICP-MS result of the NAC catalyst.

Elements	Content (wt%)	Elements	Content (wt%)	Elements	Content (wt%)
Li	0.00	Ge	0.00	Nd	0.00
Be	0.00	As	0.00	Sm	0.00
B	0.00	Se	0.00	Eu	0.00
Na	0.03	Rb	0.00	Gd	0.00
Mg	0.00	Sr	0.00	Tb	0.00
Al	0.00	Y	0.00	Dy	0.00
Si	0.97	Zr	0.00	Ho	0.00
K	0.00	Nb	0.00	Er	0.00
Ca	0.00	Mo	0.00	Tm	0.00
Sc	0.00	Ru	0.00	Yb	0.00
Ti	0.00	Rh	0.00	Lu	0.00
V	0.00	Pd	0.00	Hf	0.00
Cr	0.00	Ag	0.00	Ta	0.00
Mn	0.00	Cd	0.00	W	0.00
Fe	0.00	In	0.00	Re	0.00
Co	0.00	Sn	0.00	Os	0.00
Ni	0.00	Sb	0.00	Ir	0.00
Cu	0.00	Te	0.00	Pt	0.00
Zn	0.00	Cs	0.00	Au	0.00
Ga	0.00	Ba	0.00	Hg	0.00
		La	0.00	Tl	0.00
		Ce	0.00	Pb	0.00
		Pr	0.00	Bi	0.00
				Th	0.00
				U	0.00

Table S2 Comparison of catalytic performance for ethylbenzene dehydrogenation over reported carbon-based catalysts.

Entry	Catalysts	W_{cat}[a] (mg)	Temp.[b] (°C)	Veloc.[c] ($mL \cdot min^{-1}$)	Conc.[d] (%)	Sele.[e] (%)	Rate[f] ($mmol \cdot g^{-1} \cdot h^{-1}$)
1	ND@NMC/SiC[9]	300	600	30	2.8	96	9.9
2	ND/CNT-SDS[10]	25	550	10	2.8	98.2	7.7
3	ND/NCMS−NCP_{ImM}[11]	50	550	30	2.8	99.5	7.12
4	ND/CN-ms-o[12]	25	550	10	2.8	99.8	7.06
5	granule ND@NC[13]	25	550	10	2.8	99	6.39
6	ND-@NMC[14]	150	550	30	2.8	99.6	5.8
7	N,O-ND/CNT-d[15]	25	550	10	2.8	98.7	5.2
8	N-RGO/ND[16]	25	550	10	2.8	97.2	4.94
9	MN-CNT[17]	25	550	10	2.8	98.4	4.8
10	H-ND[18]	25	550	10	2.8	95.8	4.8
11	NCMS@NC_{glu}-NH_4Cl[19]	25	550	10	2.8	96.4	4.77
12	HN-CNT[20]	25	550	10	2.8	98.5	4.6
13	M-Glu-CNT[21]	25	550	10	2.8	98	4.6
14	MCSA-CNT[22]	25	550	10	2.8	98	4.5
15	G-M-CNT-750[23]	25	550	10	2.8	99	4.34
16	ND/CN_x-750[24]	25	550	10	2.8	99	4
17	A-M-CNT[25]	25	550	10	2.8	98.5	4
18	DUT-1-750[26]	25	550	10	2.8	93.8	3.45
19	ND[27]	25	550	10	2.8	98.4	2.99
20	20-MgO-rGO[28]	50	550	10	2.6	98.2	2.946
21	N-CNT-AC[29]	25	550	10	2.8	94.7	2.46
22	N−C/CNT-$N_{15.3}$[30]	300	550	30	2.8	99	2.22
23	ND/NCF-FLG[31]	300	550	30	2.8	96.4	2.03
24	ND-FLG[32]	300	550	30	2.8	99	1.95
25	NMCS[33]	100	550	10	2.8	85	1.75
26	N-C[34]	50	550	20	2	99	1.62
27	HD-ND/graphene$_{(4wt\%)}$[35]	50	550	10	2.6	97.5	1.46
28	NPCB-900[36]	300	550	30	3.1	93.2	1.2
29	ND/CNT-SiC[37]	500	550	10	2.6	98.3	0.3
30	NAC[g]	20	550	100	2.4	99	6.0
31	NAC[g]	20	300	50	0.24	99	0.2

[a] Catalyst loading. [b] Reaction temperature. [c] The total volume velocity of the feed. [d] Concentration of ethylbenzene. [e] Styrene selectivity. [f] Steady-state styrene formation rate. [g] This work.

Section 3. Supplementary References

[1] Z. Luo, R. Nie, V. T. Nguyen, A. Biswas, R. K. Behera, X. Wu, T. Kobayashi, A. Sadow, B. Wang, W. Huang, *Nature Communications* **2020**, *11*, 4091.

[2] aH. Nies, H. Bauer, K. Roth, D. Rewicki, *Journal of Magnetic Resonance (1969)* **1980**, *39*, 521-524; bT. Schaefer, G. H. Penner, R. Sebastian, *Canadian Journal of Chemistry* **1987**, *65*, 873-877.

[3] G. Kresse, J. Furthmüller, *Physical review B* **1996**, *54*, 11169.

[4] J. P. Perdew, K. Burke, M. Ernzerhof, *Physical review letters* **1996**, *77*, 3865.

[5] aP. E. Blöchl, *Physical review B* **1994**, *50*, 17953; bG. Kresse, D. Joubert, *Physical review b* **1999**, *59*, 1758.

[6] B. Wang, L. Tsetseris, S. T. Pantelides, *Journal of Materials Chemistry A* **2013**, *1*, 14927-14934.

[7] S. Li, T. Mou, G. Ren, J. Warzywoda, Z. Wei, B. Wang, Z. Fan, *Journal of Materials Chemistry A* **2017**, *5*, 1650-1657.

[8] aG. Henkelman, B. P. Uberuaga, H. Jónsson, *The Journal of chemical physics* **2000**, *113*, 9901-9904; bG. Henkelman, H. Jónsson, *The Journal of chemical physics* **1999**, *111*, 7010-7022.

[9] H. Ba, J. Luo, Y. Liu, C. Duong-Viet, G. Tuci, G. Giambastiani, J.-M. Nhut, L. Nguyen-Dinh, O. Ersen, D. S. Su, C. Pham-Huu, *Applied Catalysis B: Environmental* **2017**, *200*, 343-350.

[10] Q. Zhou, Z. Zhao, *ChemCatChem* **2019**, *12*, 342-349.

[11] X. Wei, G. Ge, W. Yu, H. Guo, X. Guo, C. Song, Z. Zhao, *ACS Appl Mater Interfaces* **2022**, *14*, 19315-19323.

[12] G. Ge, X. Guo, C. Song, Z. Zhao, *Catalysis Science & Technology* **2020**, *10*, 1048-1055.

[13] Q. Zhou, G. Ge, Z. Guo, Y. Liu, Z. Zhao, *ACS Catalysis* **2020**, *10*, 14604-14614.

[14] Y. Liu, H. Ba, J. Luo, K.-H. Wu, J.-M. Nhut, D. S. Su, C. Pham-Huu, *Catalysis Today* **2018**, *301*, 38-47.

[15] Q. Zhou, X. Guo, C. Song, Z. Zhao, *ACS Applied Nano Materials* **2019**, *2*, 2152-2159.

[16] Z. Zhao, Y. Dai, G. Ge, Q. Mao, Z. Rong, G. Wang, *ChemCatChem* **2015**, *7*, 1070-1077.

[17] Z. Zhao, Y. Dai, G. Ge, X. Guo, G. Wang, *Green Chemistry* **2015**, *17*, 3723-3727.

[18] Z. Zhao, W. Li, Y. Dai, G. Ge, X. Guo, G. Wang, *ACS Sustainable Chemistry & Engineering* **2015**, *3*, 3355-3364.

[19] G. Ge, H. Liu, Z. Zhao, *ChemCatChem* **2019**, *11*, 4830-4840.

[20] Z. Zhao, Y. Dai, G. Ge, X. Guo, G. Wang, *RSC Advances* **2015**, *5*, 53095-53099.

[21] Z. Zhao, Y. Dai, G. Ge, G. Wang, *AIChE Journal* **2015**, *61*, 2543-2561.

[22] Z. Zhao, Y. Dai, G. Ge, G. Wang, *Chemistry* **2015**, *21*, 8004-8009.

[23] Z. Zhao, Y. Dai, G. Ge, G. Wang, *ChemCatChem* **2015**, *7*, 1135-1144.

[24] Z. Zhao, Y. Dai, *J. Mater. Chem. A* **2014**, *2*, 13442-13451.

[25] Z. Zhao, Y. Dai, G. Ge, X. Guo, G. Wang, *Phys Chem Chem Phys* **2015**, *17*, 18895-18899.

[26] Z. Zhao, Y. Dai, J. Lin, G. Wang, *Chemistry of Materials* **2014**, *26*, 3151-3161.

[27] G. Ge, Z. Zhao, *Applied Catalysis A: General* **2019**, *571*, 82-88.

[28] J. Diao, Y. Zhang, J. Zhang, J. Wang, H. Liu, D. S. Su, *Chem Commun (Camb)* **2017**, *53*, 11322-11325.

[29] Z. Zhao, Y. Dai, G. Ge, *Catalysis Science & Technology* **2015**, *5*, 1548-1557.

[30] H. Ba, Y. Liu, L. Truong-Phuoc, C. Duong-Viet, J.-M. Nhut, D. L. Nguyen, O. Ersen, G. Tuci, G. Giambastiani, C. Pham-Huu, *ACS Catalysis* **2016**, *6*, 1408-1419.
[31] H. Ba, L. Truong-Phuoc, Y. Liu, C. Duong-Viet, J.-M. Nhut, L. Nguyen-Dinh, P. Granger, C. Pham-Huu, *Carbon* **2016**, *96*, 1060-1069.
[32] H. Ba, S. Podila, Y. Liu, X. Mu, J.-M. Nhut, V. Papaefthimiou, S. Zafeiratos, P. Granger, C. Pham-Huu, *Catalysis Today* **2015**, *249*, 167-175.
[33] J. Wang, H. Liu, J. Diao, X. Gu, H. Wang, J. Rong, B. Zong, D. S. Su, *Journal of Materials Chemistry A* **2015**, *3*, 2305-2313.
[34] J. Shi, Y. Wei, D. Zhou, L. Zhang, X. Yang, Z. Miao, H. Qi, S. Zhang, A. Li, X. Liu, W. Yan, Z. Jiang, A. Wang, T. Zhang, *ACS Catalysis* **2022**, *12*, 7760-7772.
[35] J. Diao, H. Liu, Z. Feng, Y. Zhang, T. Chen, C. Miao, W. Yang, D. S. Su, *Catalysis Science & Technology* **2015**, *5*, 4950-4953.
[36] L. Qin, L. Wang, C. Wang, X. Yang, B. Lv, *Molecular Catalysis* **2019**, *462*, 61-68.
[37] H. Liu, J. Diao, Q. Wang, S. Gu, T. Chen, C. Miao, W. Yang, D. Su, *Chem Commun (Camb)* **2014**, *50*, 7810-7812.